

AD-A134 389

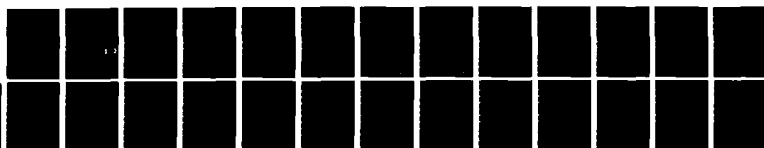
DISCHARGE KINETICS OF THE NICKEL ELECTRODE(U) AEROSPACE 1/1  
CORP EL SEGUNDO CA CHEMISTRY AND PHYSICS LAB  
A H ZIMMERMAN ET AL. 15 SEP 83 TR-0083(3945-01)-2

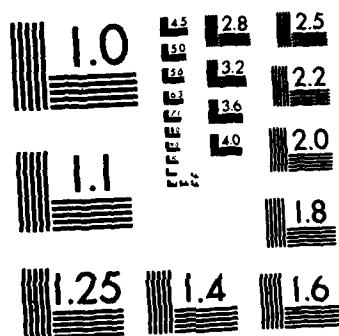
UNCLASSIFIED

SD-TR-83-61 F04701-82-C-0083

F/G 7/2

NL





MICROCOPY RESOLUTION TEST CHART  
NATIONAL BUREAU OF STANDARDS-1963-A

12

AD-A134 389

## Discharge Kinetics of the Nickel Electrode

A. H. ZIMMERMAN and P. K. EFFA  
Chemistry and Physics Laboratory  
The Aerospace Corporation  
El Segundo, Calif. 90245

15 September 1983

DTIC  
ELECTE  
NOV 4 1983  
S B D

APPROVED FOR PUBLIC RELEASE;  
DISTRIBUTION UNLIMITED

DTIC FILE COPY

Prepared for  
SPACE DIVISION  
AIR FORCE SYSTEMS COMMAND  
Los Angeles Air Force Station  
P.O. Box 92960, Worldway Postal Center  
Los Angeles, Calif. 90009

83 10 31 015

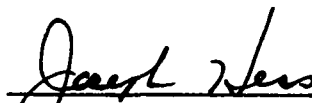
This report was submitted by The Aerospace Corporation, El Segundo, CA 90245, under Contract No. F04701-82-C-0083 with the Space Division, P.O. Box 92960, Worldway Postal Center, Los Angeles, CA 90009. It was reviewed and approved for The Aerospace Corporation by S. Feuerstein, Director, Chemistry and Physics Laboratory. Captain James C. Garcia, WCO, AFSTC, was the project officer for the Mission Oriented Investigation and Experimentation Program.

This report has been reviewed by the Public Affairs Office (PAS) and is releasable to the National Technical Information Service (NTIS). At NTIS, it will be available to the general public, including foreign nationals.

This technical report has been reviewed and is approved for publication. Publication of this report does not constitute Air Force approval of the report's findings or conclusions. It is published only for the exchange and stimulation of ideas.



James C. Garcia, Captain, USAF  
Project Officer



Joseph Hess, GM-15, Director  
West Coast Office, AF Space Technology  
Center

UNCLASSIFIED

SECURITY CLASSIFICATION OF THIS PAGE (When Data Entered)

REPORT DOCUMENTATION PAGE		READ INSTRUCTIONS BEFORE COMPLETING FORM
1. REPORT NUMBER SD-TR- 83-61	2. GOVT ACCESSION NO. AD-A134384	3. RECIPIENT'S CATALOG NUMBER
4. TITLE (and Subtitle)  DISCHARGE KINETICS OF THE NICKEL ELECTRODE		5. TYPE OF REPORT & PERIOD COVERED
		6. PERFORMING ORG. REPORT NUMBER TR-0083(3945-01)-2
7. AUTHOR(s) A. H. Zimmerman and P. K. Effa		8. CONTRACT OR GRANT NUMBER(s) F04701-82-C-0083
9. PERFORMING ORGANIZATION NAME AND ADDRESS  The Aerospace Corporation El Segundo, Calif. 90245		10. PROGRAM ELEMENT, PROJECT, TASK AREA & WORK UNIT NUMBERS
11. CONTROLLING OFFICE NAME AND ADDRESS Space Division Air Force Systems Command Los Angeles, Calif. 90009		12. REPORT DATE 15 September 1983
		13. NUMBER OF PAGES 22
14. MONITORING AGENCY NAME & ADDRESS (if different from Controlling Office)		15. SECURITY CLASS. (of this report) Unclassified
		15a. DECLASSIFICATION/DOWNGRADING SCHEDULE
16. DISTRIBUTION STATEMENT (of this Report)  Approved for public release; distribution unlimited.		
17. DISTRIBUTION STATEMENT (of the abstract entered in Block 20, if different from Report)		
18. SUPPLEMENTARY NOTES		
19. KEY WORDS (Continue on reverse side if necessary and identify by block number) nickel electrode battery impedance kinetics cell		
20. ABSTRACT (Continue on reverse side if necessary and identify by block number)  The kinetics of nickel electrode discharge are found to be controlled by solid-state proton diffusion under normal high rate discharge conditions. As the nickel electrode is discharged, the conductivity of the active material decreases until eventually mixed kinetics are observed where the electrode impedance has significant contributions from both proton diffusion and charge transfer resistance. Further discharge results		

UNCLASSIFIED

SECURITY CLASSIFICATION OF THIS PAGE(When Data Entered)

19. KEY WORDS (Continued)

20. ABSTRACT (Continued)

in the formation of a semiconductor layer at the metal-active material interface that is depleted in charge carriers and has a relatively high electronic resistance. The depletion layer is responsible for the secondary discharge plateau of the nickel electrode at 0 to -0.5 volts vs. Hg/HgO. Changes in electrode capacitance during depletion layer formation appear to provide a sensitive measure of the uniformity of electrode discharge. The effects of cobalt additives on the kinetics have been experimentally measured, and while cobalt does not change the discharge mechanism, it does increase the ionic and electronic conductivity of the active material allowing a greater depth of discharge before depletion layer formation.

UNCLASSIFIED

SECURITY CLASSIFICATION OF THIS PAGE(When Data Entered)

# CONTENTS

PREFACE.....	5
I. INTRODUCTION.....	7
II. EXPERIMENTAL.....	9
III. NICKEL ELECTRODE DISCHARGE KINETICS.....	11
A. Results.....	11
B. Discussion of Nickel Electrode Kinetics.....	16
C. Electrode Capacitance and Nonuniformities.....	18
D. Cobalt Additive Effect.....	22
REFERENCES.....	25



Accession For	
NTIS DTIC	<input checked="" type="checkbox"/>
DTIC TAR	<input type="checkbox"/>
Unannounced	<input type="checkbox"/>
Justification	
<b>PER CALL JC</b>	
By	
Distribution/	
Availability Codes	
Dist	Avail and/or Special
<b>A-1</b>	

## FIGURES

1.	Discharge Voltage of a Sintered Nickel Electrode at C/10 Rate Followed by a C/100 Discharge of Residual Capacity.....	12
2.	Transient Impedance Measurements at Points a, b, and c During the Discharge of Fig. 1.....	13
3.	Resistance R as a Function of Voltage During C/100 Discharge of the Residual Capacity in a Sintered Nickel Electrode.....	14
4.	Sintered Nickel Electrode Capacitance.....	15
5.	Capacitance of Nickel Electrodes During a C/100 Discharge of Residual Capacity.....	20
6.	Mott-Schottky Plots for Sintered and Flat Plate Nickel Electrodes.....	21
7.	Resistance R as a Function of Voltage for a Nickel Electrode.....	23





## PREFACE

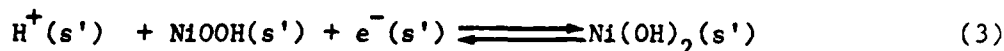
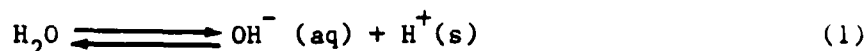
The support of the Space Division of the United State Air Force is gratefully acknowledged (Contract No. F04701-81-C-0082). We also wish to thank P. Riley for invaluable technical assistance in the chemical analysis of the electrodes.



## I. INTRODUCTION

The oxidation/reduction reactions at the nickel electrode have been the subject of a number of studies during recent years. As more experimental studies have been reported, it has become clear that the electrochemistry of the nickel electrode is quite complex. The early work of Bode, Dehmelt, and Witte, (Ref. 1) and the later work of others, (Ref. 2) indicated the existence of both  $\alpha$  and  $\beta$  phases of  $\text{Ni}(\text{OH})_2$ . These two phases may be oxidized to  $\gamma$  and  $\beta$  phases of nickel oxyhydroxide respectively, and may also undergo chemical interconversion. Additional energetically discernable phases have been found in the work of Schrebler-Guzman et al., (Ref. 3) and Barnard et al. (Ref. 4). In light of the growing number of possible phase structures it is anticipated that the kinetics of the nickel electrode oxidation/reduction processes will be difficult to unravel, particularly in sintered nickel electrodes where the effects of additives and phase nonuniformities are expected to provide additional kinetic and thermodynamic complexity.

Nickel electrode reduction has been found to follow diffusion kinetics in a number of previous studies (Refs. 5-8). The limiting diffusion process in the voltage range above 0.2 volts (vs.  $\text{Hg}/\text{HgO}$ ) is the diffusion of protons formed at the electrode/electrolyte interface to the charge-transfer site. The reduction process may be represented as



Reaction (1) represents the formation of a proton at catalytic site s at the electrode/electrolyte interface; reaction (2) involves diffusion of the proton from site s into the electrode to the charge-transfer site s'; and reaction (3) is the charge transfer process involving the reduction of one of the



higher valency species of active material in the lattice, represented here as simply  $\text{NiOOH}$ . Reactions (1) and (3) are not generally believed to be rate-limiting under the operating conditions of the nickel electrode because they would not account for the observed diffusion kinetics. A recent report (Ref. 9) that reaction (1) may be rate-limiting appears to be more consistent with diffusion of  $\text{OH}^-$  between the bulk electrolyte and the active material surface as the rate-limiting step for high rate electrode operation, particularly at reduced concentrations of  $\text{OH}^-$ . Reaction (2), proton diffusion, is generally regarded as controlling the rate of nickel electrode discharge at the potential and current densities normally used in battery operation. Barnard (Ref. 10) has obtained electrochemical evidence that the protons involved in processes (1)-(3) are delocalized throughout the active material lattice, a result that is consistent with spectroscopic data in which the lack of IR absorption bands due to OH in the oxidized active material is reported (Ref. 11). The proton diffusion rate and proton concentration are expected to depend on the phase composition of the  $\text{NiOOH}$ , as well as on the presence of additives in the lattice structure (Ref. 8).

During normal discharge of the nickel electrode in a battery cell the diffusion process indicated by reaction (2) is rate-limiting. However, for some conditions of electrode structure (Ref. 13) or operation (Ref. 12), the electrode voltage can prematurely drop to a plateau at 0 to -0.5 volts (vs.  $\text{Hg/HgO}$ ) and the electrode can discharge a substantial portion of its capacity at the lower potential. The lower voltage discharge has been attributed to effects such as adsorbed oxygen, (Refs. 14-17) lower energy nickel oxides, (Refs. 18-22) and conductivity changes (Refs. 13,23). Measurements of the electrode kinetics in the low state of charge region should allow the process(es) causing the low discharge voltage plateau to be identified. Such measurements of the electrochemical kinetics of the nickel electrode are reported here. The kinetics are measured over a wide range of electrode potential for electrodes of flat plate and sintered construction, with and without cobalt additives. The work described here provides evidence indicating that conductivity changes, coupled with the formation of an interfacial loss layer, are responsible for the premature depletion of nickel electrode capacity at voltages sufficient for battery operation.

## II. EXPERIMENTAL

Nickel electrodes were made by electrochemical deposition (Ref. 24) of  $\text{Ni(OH)}_2$  on either  $4 \text{ cm}^2$  flat nickel plates or  $1 \text{ cm}^2$  sintered nickel substrates. The nickel sinter substrate used was 0.076 cm thick and had a porosity of 79.5%. Cathodic deposition at 4 and 35  $\text{mA/cm}^2$  was used for the flat plate and sintered electrodes, respectively, using a boiling solution 60% in 2M  $\text{Ni(NO}_3)_2$  and 40% in ethanol. Cobalt nitrate was added to the solution to give the desired Ni/Co ratio for studying the effects of cobalt additives. Chemical deposition in a sintered electrode was done by repetitively evacuating the air from the sinter while dipped in a 2M  $\text{Ni(NO}_3)_2$  solution and then dipping in a 20% KOH solution. About  $0.1 \text{ g/cm}^2$  of  $\text{Ni(OH)}_2$  was typically deposited on the sintered electrode ( $1.60 \text{ g/cc}$  void), and about  $6 \text{ mg/cm}^2$  was typically deposited on the flat plate electrodes. All electrodes were cycled prior to experimental use until the capacity stabilized, which was typically 5 complete charge/discharge cycles. Rated capacities, which will be referred to, were  $20 \text{ mAh/cm}^2$  and  $0.14 \text{ mAh/cm}^2$  for sintered and flat plate electrodes, respectively.

Electrode charge and discharge, impedance measurements, and capacitance monitoring were done automatically using a computer which continuously monitored electrode voltage and controlled the current passing through the electrode. An operational amplifier power supply having a 10 kHz frequency response was used to charge and discharge the electrodes. The electrodes were monitored in a nitrogen-purged polystyrene test cell that incorporated a nickel sheet counterelectrode, a Hg/HgO reference electrode, and 31% KOH electrolyte. Electrode capacitance could be monitored by the computer through the application of a current step, the capacitance being obtained from the ratio of the magnitude of the current step to the initial slope of the electrode voltage response. Electrode capacitance was only measured at potentials where the initial voltage response to a current step was exponential in time; in potential regions where diffusion dominates the electrode kinetics capacitance measurements are meaningless. The computer similarly measured the

electrode impedance by monitoring the time dependence of the voltage response to a small current step. The method for obtaining the impedance from such transient data has been previously described (Ref. 25). The time resolution for such transient acquisition was 1 msec. All transient voltage responses for both capacitance and impedance measurements were less than 5 mV in amplitude. Digital filtering of the amplified voltage response gave a typical noise level of less than 25  $\mu$ V in the electrode voltage. Capacitance measurements could be automatically done during electrode discharge with a typical accuracy of  $\pm 0.5\%$ . All experiments were done at room temperature,  $23 \pm 2^\circ\text{C}$ .

### III. NICKEL ELECTRODE DISCHARGE KINETICS

#### A. RESULTS

The Ni electrode voltage typically follows the curve indicated in Fig. 1 when it is discharged first at C/10, then at a lower rate (C/100). The points a, b, and c indicated in Fig. 1 are the points during discharge at which the measurements in Fig. 2 were made. Figure 2 indicates the kinetic response of this electrode to a small current step at the upper voltage plateau during high rate discharge (point a), during low rate discharge (point b), and on the lower voltage plateau (point c). Also included in Fig. 2 are the electrode impedances calculated from the data at points a, b, and c during discharge. As has been found by other workers (Refs. 6-8), the kinetics are diffusion-controlled during discharge on the upper voltage plateau at point a. Diffusion control is indicated by the linear region in the plot of transient voltage vs  $\sqrt{t}$  in Fig. 2 at point a, or similarly by the linear dependence rising from the origin with a 45° slope in the impedance plot of Fig. 2 at point a. The electrode at point b, while still discharging on the upper voltage plateau, exhibits mixed kinetics suggestive of both activation and diffusion-controlled processes influencing the discharge. At point c on the lower plateau the discharge kinetics are dominated by an activation-controlled process. Activation kinetics are characterized by an exponential transient response in time which gives a semicircular impedance plot as shown in Fig. 2 for point c. In the discussion that follows, the resistance and capacitance associated with the activation-controlled processes at points b and c will be labeled R and C, respectively. The diffusion resistance associated with the diffusion-controlled process at points a and b in Fig. 1 will be referred to as  $R_d$ .

Both R and C were measured during constant current discharge as a function of potential and state of charge. These results are indicated in Figs. 3 and 4, respectively. In Fig. 3, log R is plotted vs potential during the course of a C/100 discharge. Also, at various times during the discharge in Fig. 3 the current was varied so as to allow measurement of R as a function of voltage at a constant oxidation state. The plot of capacitance as a function

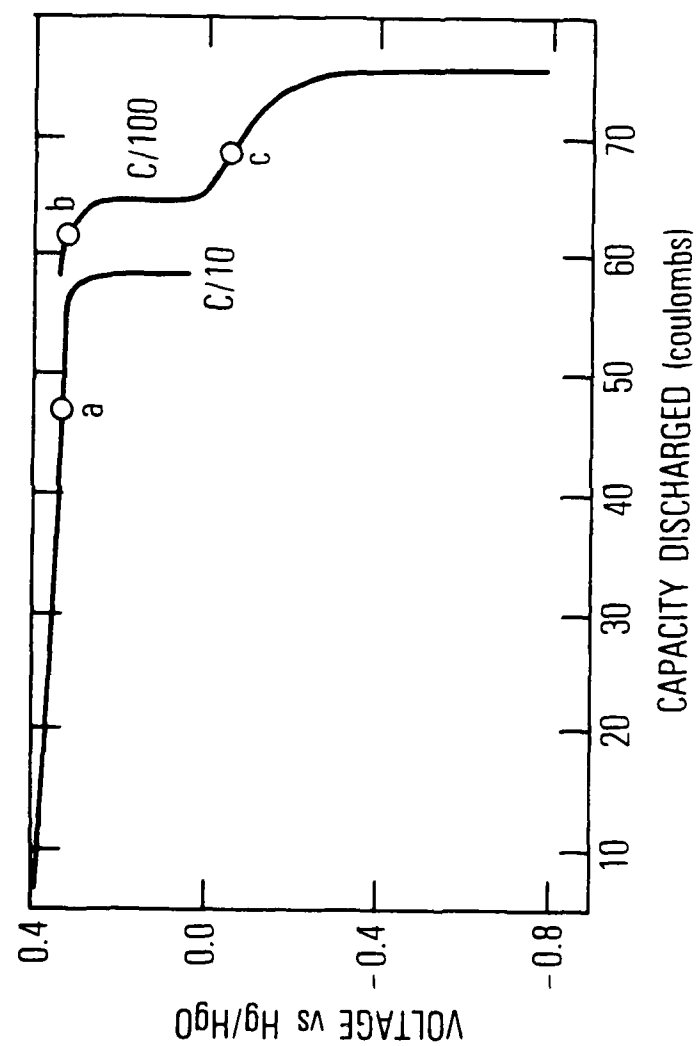


Fig. 1. Discharge voltage of a sintered nickel electrode at C/10 rate followed by a C/100 discharge of residual capacity. The points a, b, and c refer to measurement points in Fig. 2.

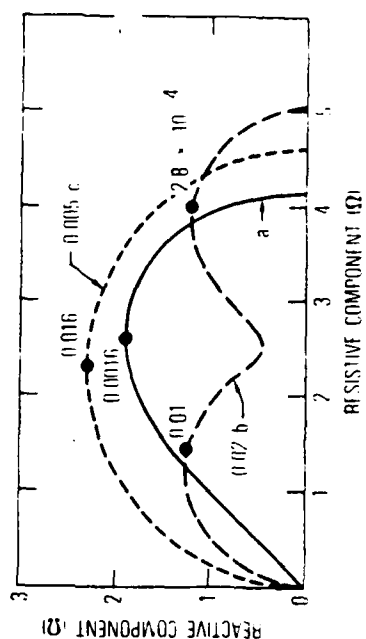
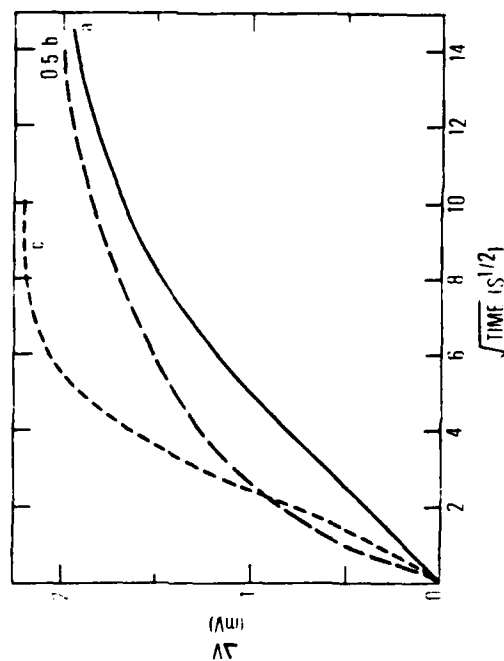


Fig. 2. Transient impedance measurements at points, a, b, and c during the discharge of Fig. 1. The curves on the left are the transient responses to current changes and the curves on the right are the impedances calculated from the time transients. The numbers indicate the frequencies of the reactive extrema in Hz. The multipliers indicated have been applied to both coordinates.



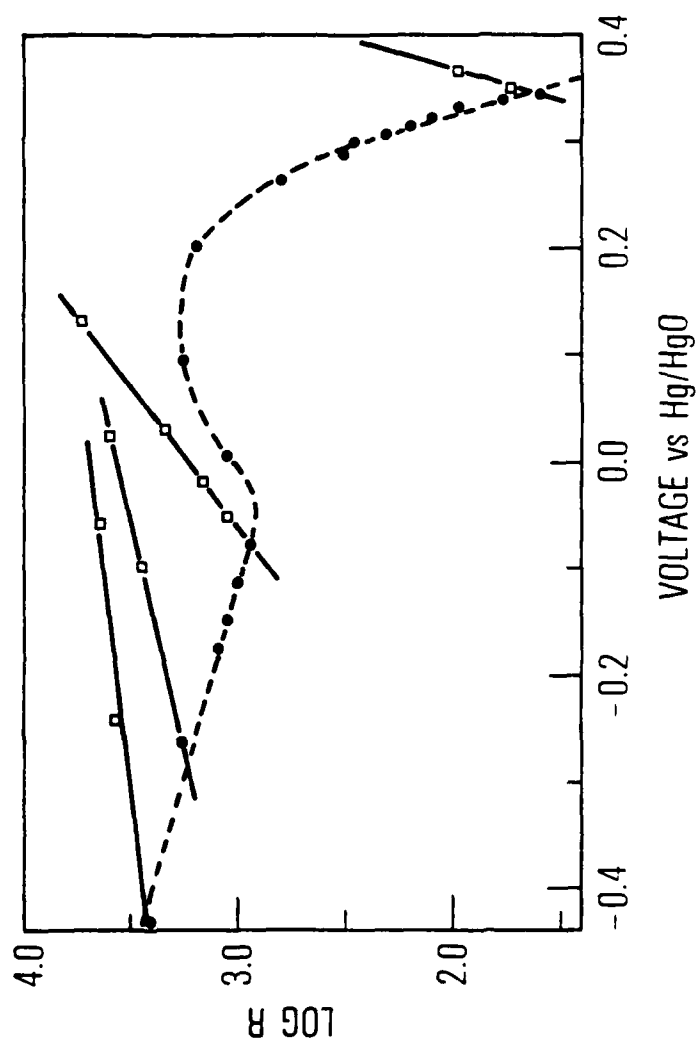


Fig. 3. Resistance  $R$ , as a function of voltage (solid circles) during C/100 discharge of the residual capacity in a sintered nickel electrode. At various times during the C/100 discharge the resistance was measured as a function of potential as indicated by the solid lines.

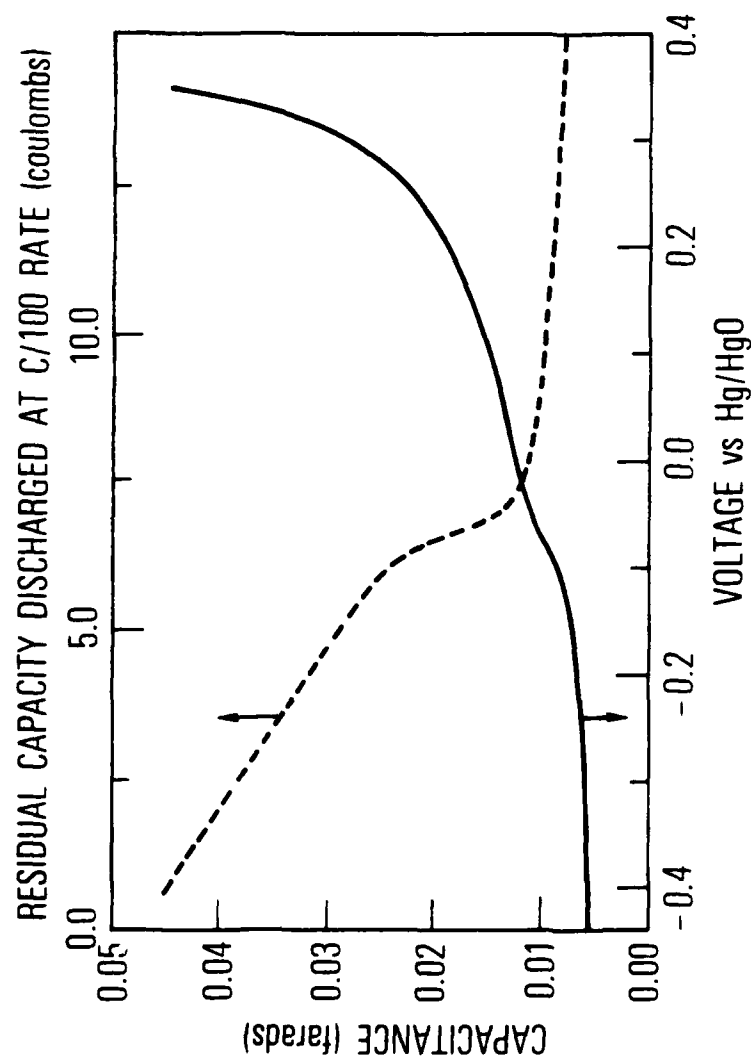


Fig. 4 Sintered nickel electrode capacitance as a function of voltage (solid line) and capacity discharged (dashed line) during discharges of residual capacity at C/100 rate.

of voltage in Fig. 4 did not change significantly as the oxidation state of the electrode decreased. The dependence of the capacitance on the residual capacity  $Q$  discharged from the electrode is also indicated in Fig. 4. The capacitance decreases linearly with  $Q$  until the lower voltage plateau is reached, after which the capacitance is relatively constant during further discharge.

The results indicated in Figs. 1 to 4 are for an electrochemically impregnated sintered nickel electrode. Similar results were obtained for chemically deposited active material. Flat plate electrodes also gave similar behavior in that diffusion-controlled kinetics changed into mixed kinetics, and then finally into activation-controlled kinetics as the electrode was discharged. For the flat plate electrodes the current density was scaled down to realize a  $C/10$  or a  $C/100$  rate.

#### B. DISCUSSION OF NICKEL ELECTRODE KINETICS

Three processes have been observed that can control reduction rates at the nickel electrode. The diffusion kinetics that are observed above 0.3 volts are consistent with previous results attributed to proton diffusion in Ni electrodes (Refs. 6-8) and in the NiCd cell (Ref. 25). For a flat plate electrode, proton diffusion coefficients of about  $10^{-10} \text{ cm}^2 \text{ s}^{-1}$  are obtained from the measured diffusion times, assuming a film thickness proportional to capacity (about  $10^{-4} \text{ cm}$ ). Deviations from ideal diffusion-controlled behavior are observed at high currents ( $> C/2$ ) and also above about 70% state of charge. It is possible that these deviations are due to nonuniform ionic conduction within the active material; for example, proton diffusion should be predominantly along grain boundaries at the beginning of discharge when reaction is largely at the grain surfaces. The impedance arising from electrolyte diffusion in the pore structure of the sintered electrodes was not significant relative to the solid-state proton diffusion impedance at the discharge rates employed here, but does become significant at higher rates. This conclusion is supported by the similar impedance characteristics measured for flat plate and porous electrodes.

While still on the upper voltage plateau, but at low states of charge, a second process begins to control the kinetics, as indicated by the mixed kinetics at point b in Figs. 1 and 2. This process is activation-controlled and as shown in Fig. 3 has a Tafel slope of about 60 mV/decade. The same slope was observed for all electrodes studied; flat plate electrodes, sintered electrodes, and electrodes in commercial NiCd cells. The slope is consistent with the single electron transfer process given by reaction (3) becoming rate-limiting. Also, because the capacitance decreases linearly with charge transfer site density or electrode state of charge in the region above 0.2 volts, reaction (3) appears most likely to control the rate. Therefore, in the region having about a 60 mV/decade Tafel slope, the density of charge transfer sites appears to have decreased to the level where charge transfer has become rate-limiting. Discharge in this region continuously decreases the density of higher valency sites and thereby increases the charge transfer resistance of the active material. It should also be noted that the open circuit voltage of the active material continuously decreases as the density of higher valency sites diminishes.

As the Ni electrode is discharged towards the divalent state, a third process can cause the electrochemical kinetics to change dramatically in the potential range between 0.1 and 0.2 volts. While the active material above 0.2 volts acts as an electronic conductor, below 0.2 volts a layer of active material begins to behave like a semiconductor, exhibiting Tafel slopes (Fig. 3) that continuously increase as the material is reduced. The sudden decrease in capacitance that accompanies the transition to the lower voltage plateau (Fig. 4) is consistent with the formation of a layer of carrier-depleted material at the metal current-collector/active material interface, such that the resistance and capacitance of this layer now dominate the discharge kinetics. Continued discharge on the lower voltage plateau causes the depletion layer to grow in thickness (and resistance) towards the solution interface.

The model presented above is similar to models put forth qualitatively by Klapste et al. (Ref. 13) and somewhat more quantitatively by Barnard, et al., (Ref. 23), in that changes in the conductivity of the active material cause

the lower voltage plateau. The model of Barnard, et al. (Ref. 23) fits the Tafel slope reported here on the upper voltage plateau. However the Tafel slopes observed on the lower voltage plateau suggest that a poorly conducting semiconducting layer has formed and that the electrode overpotential arises from the space charge voltage across the layer. The layer is kinetically maintained by current flow and it is therefore expected that both its thickness and its conductivity at a given state of charge will depend on current density. The kinetics on the lower plateau are clearly activation-controlled, indicating that conduction through the depleted layer does not occur through ionic migration.

While it is technically true that a secondary plateau in the voltage is not observed during recharge of a Ni electrode, the increased resistance associated with the depletion layer can be clearly seen in the early stages of Ni electrode oxidation. After generation of a depletion layer by a low rate discharge to low potentials, the electrode voltage goes through an initial high voltage peak when recharge is initiated. It has been well established that after shorting NiCd cells down for long periods, recharge must be initiated at quite a low rate to keep the voltage from initially rising to unacceptably high levels. Such a voltage peak is likely to arise from the ohmic contribution of the depletion layer, which can become quite thick in instances of long term cell short-down.

### C. ELECTRODE CAPACITANCE AND NONUNIFORMITIES

The model described above for the kinetics of the nickel electrode suggests that above about 0.25 V the capacitance of the electrode is controlled by the density of higher valency sites available for reduction, giving the linear relationship between capacitance and residual capacity in Fig. 4 below 6 coulombs (above 0.25 volts). Continued discharge to the lower voltage plateau causes a drop in capacitance as it becomes controlled by the space charge capacitance across the depleted layer at the active material/current collector interface. The drop in capacitance should be sensitive to the structure of the active material at this interface. A low interfacial contact area (high interfacial current density) should give a

greater drop in capacitance, and any energetic differences in active material at the current collector interface should spread the capacitance drop over a range of discharge capacity and thereby decrease the sharpness of the drop. The manner in which the capacitance varies during discharge of residual capacity can therefore indicate the causes for changes or differences in electrode performance. In Fig. 5 plots of electrode capacitance as a function of residual capacity are shown for a sintered nickel electrode after being cycled 32 times, after being reconditioned, and for a flat plate nickel electrode. The most striking difference between the electrodes is the degree of sharpness of the capacitance drop as electrode voltage drops to the lower discharge plateau. For the sintered electrode that has been cycled many times the active material at the current collector interface has developed significant nonuniformities which are likely to be associated with energetic variations between different phases or structures of the active material at the interface. The flat plate electrode, on the other hand, has an extremely sharp drop in capacitance in Fig. 5, suggesting a highly uniform active material/current collector interface. The greater relative drop in capacitance for the flat plate electrode is likely to be due to a somewhat higher interfacial current density.

The capacitance on the lower plateau, if due to a perfectly uniform semiconductor layer, would be expected to exhibit a Mott-Schottky dependence on voltage. This relationship is plotted in Fig. 6 for differing amounts of residual capacity discharged for both sintered and flat plate electrodes. At all states of discharge the relationship is essentially linear above 0 volts for the flat plate electrode, and above 0.05 volts for the sintered electrodes. The linear ranges are not large because data only extend up to about 0.15 volts since the depleted layer cannot be maintained above this voltage under galvanostatic conditions. It is interesting to note that for all states of discharge for both the flat plate and the sintered electrodes, the higher voltage data extrapolate to 0.32 volts vs. Hg/HgO. A possible explanation for the linear behavior at higher voltages and the pronounced curvature at lower voltages is that at lower voltages the depleted layer

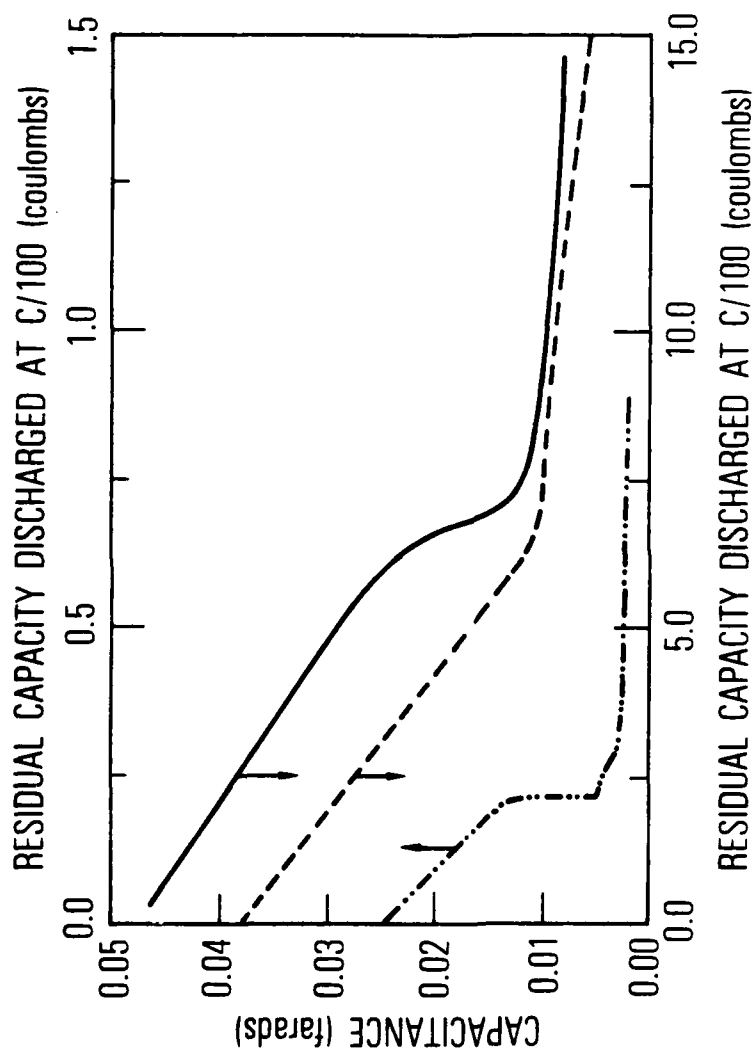


Fig. 5. Capacitance of nickel electrodes during a C/100 discharge of residual capacity. The solid curve is for an uncycled 1 cm<sup>2</sup> sintered electrode after formation, dashed curve for a 1 cm<sup>2</sup> sintered electrode after 32 cycles, and the dash-dot curve is for an uncycled 4 cm<sup>2</sup> flat plate nickel electrode.

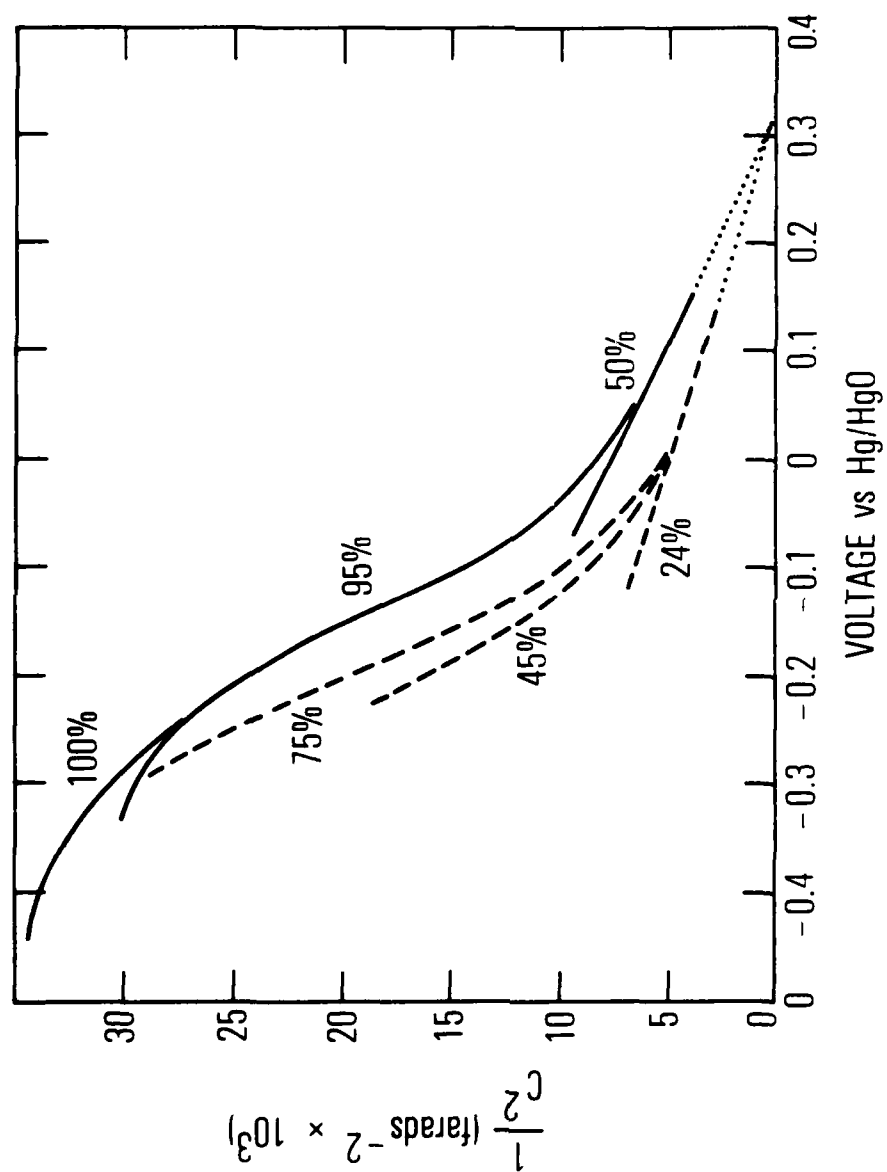


Fig. 6 Mott-Schottky plots for sintered (solid lines) and flat plate (dashed lines) nickel electrodes at various points of discharge of residual capacity. The percentages of residual capacity discharged are indicated. For the flat electrode  $1/C_2^2$  has been scaled down by 10.



becomes quite thick relative to grain sizes and active material nonuniformities, thus giving a highly inhomogeneous space charge region. At high voltages the depleted layer is extremely thin and is therefore less likely to exhibit Mott-Schottky deviations.

#### D. COBALT ADDITIVE EFFECT

Additives such as cobalt are generally considered to significantly improve nickel electrode performance. Although the effects of additives of this kind on the mechanisms of nickel electrode operation are not completely understood, it is expected that the additives can affect both ionic and electronic conductivity of the active material. The effects of a 10% cobalt additive on the kinetics of the nickel electrode were evaluated and are given in Fig. 7. The data in Fig. 7 clearly show that the overall discharge mechanisms on the upper and lower voltage plateaus are unchanged by the Co additive. However, the Co additive has decreased the diffusion resistance during the C/100 discharge by about an order of magnitude indicating substantially increased ionic conductivity. The electronic conductivity of the active material is also increased by the higher defect concentration provided by the cobalt. As has been previously reported (Ref. 26) the increased defect concentration decreases the equilibrium electrode voltage about 70 mV which has significant effects on the rechargeability of the nickel electrode. The high peak in the resistance during the transition from the upper to the lower voltage plateau appears to be eliminated by the cobalt additive. The peak and how cobalt additives act to eliminate it are the subject of continuing study.

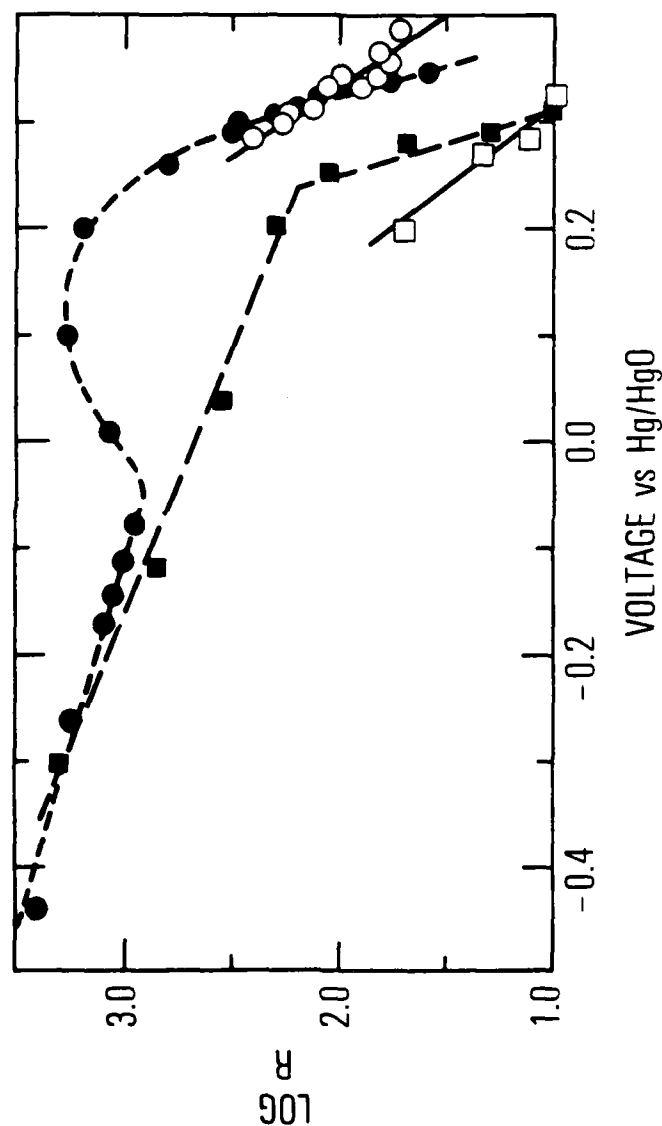


Fig. 7. Resistance  $R$  as a function of voltage for a nickel electrode (closed circles) and a nickel electrode with 10% cobalt additive (closed squares) during a C/100 discharge of residual capacity. The open symbols indicate the diffusion resistances  $R_d$ , that were also measured at the higher voltages.

# REFERENCES

1. H. Bode, K. Dehmelt, and J. Witte, Electrochim. Acta, 11, 1079 (1966).
2. R. S. Schrebler Guzman, J. R. Vilche, and A. J. Arvia, J. Applied Electrochem. 9, 183 (1979).
3. R. S. Schrebler Guzman, J. R. Vilche, and A. J. Arvia, J. Electrochem. Soc., 125, 1578 (1978).
4. R. Barnard, C. F. Randell, and F. L. Tye, J. Applied Electrochem., 10, 109 (1980).
5. D. Tuomi, J. Electrochem. Soc., 112, 371 (1965).
6. D. M. MacArthur, J. Electrochem. Soc., 117, 422 (1970).
7. D. M. MacArthur, J. Electrochem. Soc., 117, 729 (1970).
8. Z. Takehara, M. Kato, and S. Yoshizawa, Electrochim. Acta, 16, 833 (1971).
9. R. E. Carbonio, V. A. Macagno, M. C. Giordano, J. R. Vilche, and A. J. Arvia, J. Electrochem. Soc., 129 (5), 983 (1982).
10. R. Barnard, C. F. Randell, and F. L. Tye, J. Electroanal. Chem., 119, 17 (1981).
11. J. F. Jackowitz, The Nickel Electrode, Proceedings edited by R. Gunther and S. Gross, The Electrochemical Society, Inc., Pennington, NJ, Volume 82-4, 1982, p. 48.
12. R. Barnard, G. T. Crickmore, J. A. Lee, and F. L. Tye, J. Applied Electrochem., 10, 61 (1980).
13. B. Klapste, J. Mrha, K. Micka, J. Jindra, and V. Marecek, J. Power Sources, 4, 349 (1979).
14. J. Zedner, Z. Elektrochem., 11, 809 (1905); 12, 463 (1906); 13, 752 (1907).
15. S. U. Falk, J. Electrochem. Soc., 107, 662 (1960).
16. H. Bode, K. Dehmelt, and H. v. Dohren, Proc. 2nd Int. Symp. on Batteries, Brighton, 1966, Abstr. No. 6.
17. I. A. Dibrov, Elektrokhimiya, 14, 114 (1978).

18. F. Foerster, Z. Elektrochem., 13, 414 (1907); 14, 17 (1908); 14, 285 (1908).
19. O. Glemser and J. Einerhand, Z. Elektrochem., 54, 302 (1950).
20. O. Glemser and J. Einerhand, Z. Anorg. Allg. Chem., 261, 26 (1950).
21. J. A. Cherepkova, V. A. Kasyan, V. V. Sysoeva, N. N. Milyutin, and A. L. Rotinyan, Elektrokhimiya, 11, 443 (1975).
22. V. A. Kasyan, V. V. Sysoeva, N. N. Milyutin, and A. L. Rotinyan, Elektrokhimiya, 11, 1427 (1975).
23. R. Barnard, C. F. Randell, and F. L. Tye, J. Applied Electrochem. 10, 127 (1980).
24. D. F. Pickett and J. T. Maloy, J. Electrochem. Soc., 125 (7), 1026 (1978).
25. A. H. Zimmerman, M. R. Martinelli, M. C. Janecki, and C. C. Badcock, J. Electrochem. Soc., 129, 289 (1982).
26. R. Sabapathy, P. V. Vasudeva Rao, and H. V. K.-Udapa, J. Electrochem. Soc. India, 16, 135 (1967).

#### LABORATORY OPERATIONS

The Laboratory Operations of The Aerospace Corporation is conducting experimental and theoretical investigations necessary for the evaluation and application of scientific advances to new military space systems. Versatility and flexibility have been developed to a high degree by the laboratory personnel in dealing with the many problems encountered in the nation's rapidly developing space systems. Expertise in the latest scientific developments is vital to the accomplishment of tasks related to these problems. The laboratories that contribute to this research are:

Aerophysics Laboratory: Launch vehicle and reentry aerodynamics and heat transfer, propulsion chemistry and fluid mechanics, structural mechanics, flight dynamics; high-temperature thermomechanics, gas kinetics and radiation; research in environmental chemistry and contamination; cw and pulsed chemical laser development including chemical kinetics, spectroscopy, optical resonators and beam pointing, atmospheric propagation, laser effects and countermeasures.

Chemistry and Physics Laboratory: Atmospheric chemical reactions, atmospheric optics, light scattering, state-specific chemical reactions and radiation transport in rocket plumes, applied laser spectroscopy, laser chemistry, battery electrochemistry, space vacuum and radiation effects on materials, lubrication and surface phenomena, thermionic emission, photosensitive materials and detectors, atomic frequency standards, and bioenvironmental research and monitoring.

Electronics Research Laboratory: Microelectronics, GaAs low-noise and power devices, semiconductor lasers, electromagnetic and optical propagation phenomena, quantum electronics, laser communications, lidar, and electro-optics; communication sciences, applied electronics, semiconductor crystal and device physics, radiometric imaging, millimeter-wave and microwave technology.

Information Sciences Research Office: Program verification, program translation, performance-sensitive system design, distributed architectures for spaceborne computers, fault-tolerant computer systems, artificial intelligence, and microelectronics applications.

Materials Sciences Laboratory: Development of new materials: metal matrix composites, polymers, and new forms of carbon; component failure analysis and reliability; fracture mechanics and stress corrosion; evaluation of materials in space environment; materials performance in space transportation systems; analysis of systems vulnerability and survivability in enemy-induced environments.

Space Sciences Laboratory: Atmospheric and ionospheric physics, radiation from the atmosphere, density and composition of the upper atmosphere, aurorae and airglow; magnetospheric physics, cosmic rays, generation and propagation of plasma waves in the magnetosphere; solar physics, infrared astronomy; the effects of nuclear explosions, magnetic storms, and solar activity on the earth's atmosphere, ionosphere, and magnetosphere; the effects of optical, electromagnetic, and particulate radiations in space on space systems.

END

FILMED

11-83

DTIC